Study the Structure and Dynamics of Antifungal Agent Ketoconazole by CSA and Site-Specific Spin-Lattice Relaxation Time Measurements

Krishna Kishor Dey[1], Manasi Ghosh[2*]

1. *Department of Physics, Dr. Harisingh Gour Central University, Sagar-470003, Madhya-Pradesh, India*
2. *Physics Section, MMV, Banaras Hindu University, Varanasi-221005, Uttar-Pradesh, India*

*Corresponding author: *manasi.ghosh@bhu.ac.in*

Abstract: An azole antifungal agent, ketoconazole, is widely used in the treatment of mucosal fungal infections related to AIDS immunosuppression, organ transplantation, and cancer chemotherapy. The structure and dynamics of ketoconazole are thoroughly studied by chemical shift anisotropy tensor and site-specific spin-lattice relaxation time measurements. The molecular correlation time at crystallographically different carbon sites is calculated by considering that the spin-lattice relaxation mechanism for the ^{13}C nucleus is mainly governed by chemical shift anisotropy interaction and hetero-nuclear dipole-dipole coupling. The CSA parameters at the crystallographically distinct sites of ketoconazole are determined by two-dimensional phase adjusted spinning sideband (2D PASS) cross-polarization magic angle spinning (CP-MAS) solid-state NMR experiment. The site-specific spin-lattice relaxation time is measured by the Torchia CP experiment. The spin-lattice relaxation rate is slow for all the carbon nuclei sites except C2, C3, C4, C5, and C26 carbon nuclei reside on the piperazine ring and the methyl group. It suggests the close-pack arrangement of the molecule due to π-π stacking interaction. The molecular correlation time of all the carbon atoms reside on the benzene ring, 1,3-dioxolane ring, imidazole ring, and the 2,4-dichlorobenzene ring is of the order of 10^{-4} s, while it is of the order of 10^{-7} s for carbon atoms reside on the piperazine ring. The CSA parameters of the carbon nuclei on the piperazine ring (C2, C3, C4, C5), and the methyl group (C26) are very low compared to other carbon nuclei. The CSA parameters are very high for carbon nuclei reside on the benzene ring, imidazole ring, and the 2,4-

dichlorobenzene ring due to the presence of π-electrons. A huge variation of the spin-lattice relaxation time and the molecular correlation time are observed for numerous carbon nuclei situated on the side-chain of ketoconazole. The spin-lattice relaxation time varies from 500 s to 8 s, and the molecular correlation time varies in the range of 10^{-4}s to 10^{-7}s. These types of investigations portrayed the correlation between the structure and dynamics of the antifungal drug ketoconazole, which will help to develop the advanced antifungal drugs. Additionally, the CSA information of the drug molecules will be immensely useful for NMR crystallography.

1. Introduction:

The azole class compounds are the most potent antifungal drug for its lower toxicity, higher efficacy, and a broad spectrum of activity. Ketoconazole is an azole class compound and a synthetic derivative of phenylpiperazine with antifungal and antineoplastic activity. It is also considered as an antimitotic and a bacteriostatic agent for gram-positive bacteria. Ketoconazole has been used extensively in the treatment of superficial mycoses such as dermatophytosis and candidiasis.[1-4] This antifungal imidazole agent has also been used for the treatment of histoplasmosis, human systemic fungal infections, against Candida species, Cryptococcus neoformans, tinea corporis, tinea cruris, tinea manuum and tinea pedis, onychomycosis, seborrheic dermatitis.[5-16] Ketoconazole prohibits the conversion of lanosterol to ergosterol (which is required to maintain the integrity of the organism's cell membrane) by inhibiting the fungal cytochrome P450 (CYP51). Cytochrome P-450 enzyme is necessary to remove the C-14 methyl group of lanosterol.[17,18] Ketoconazole also can blockage the conversion of lanosterol to cholesterol in mammals. It can block adrenal steroidogenesis by inhibiting the corticoid 11β −hydroxylase. Because of this property, ketoconazole is used for the treatment of prostate cancer and Cushing's syndrome, respectively.[18]

Solid state NMR spectroscopy is an indispensible tool to determine the structure and dynamics of a compound. The chemical shift anisotropy (CSA) tensor is one of the most important parameter which can be measured by applying sophisticated SSNMR techniques. It can provide information about the electronic distribution, molecular orientation, and molecular dynamics surrounding a nucleus. The Larmor precession frequency of the nucleus depends on the orientation of the molecular moiety with respect to the external magnetic field and the electronic distribution around it. The shift of the precession frequency of the nucleus inside the matter is expressed as $\omega(\theta,\varphi) - \omega_0 = \omega_{iso} + (\Delta\delta/2)(3\cos^2\theta - 1 - \eta\sin^2\theta\cos2\varphi)$, where the anisotropy parameter $\Delta\delta$ measures the deviation of the electron cloud from the spherically symmetric charge distribution, and the asymmetry parameter η measures the deviation of electronic charge distribution from axially symmetric shape. In principal axis system (PAS), $\theta,$ and φ are respectively the polar and azimuthal angles with respect to the direction of the applied magnetic field($\mathbf{B_0}$).[19] The effective magnetic field experienced by the nucleus is $\mathbf{B_{eff}} = (1 \pm \delta)\mathbf{B_0}$. The dimensionless quantity δ is the chemical shift anisotropy (CSA) tensor. It is a second rank tensor with nine components.[19-26] The diagonal components of this tensor in the principal axis system (PAS) are [27,28]

$$\delta_{33} = \frac{e^2}{2m}\langle 0\left|\frac{x^2 + y^2}{r^3}\right|0\rangle - \left(\frac{e\hbar}{2m}\right)^2 \sum_n \left\{\frac{\langle 0|L_z|n\rangle\langle n\left|\frac{2L_z}{r^3}\right|0\rangle}{(E_n - E_0)} + \frac{\langle 0\left|\frac{2L_z}{r^3}\right|n\rangle\langle n|L_z|0\rangle}{(E_n - E_0)}\right\} \quad (1)$$

$$\delta_{11} = \frac{e^2}{2m}\langle 0\left|\frac{y^2 + z^2}{r^3}\right|0\rangle - \left(\frac{e\hbar}{2m}\right)^2 \sum_n \left\{\frac{\langle 0|L_x|n\rangle\langle n\left|\frac{2L_x}{r^3}\right|0\rangle}{(E_n - E_0)} + \frac{\langle 0\left|\frac{2L_x}{r^3}\right|n\rangle\langle n|L_x|0\rangle}{(E_n - E_0)}\right\} \quad (2)$$

$$\delta_{22} = \frac{e^2}{2m}\langle 0 \left| \frac{x^2 + z^2}{r^3} \right| 0\rangle$$

$$-\left(\frac{e\hbar}{2m}\right)^2 \sum_n \left\{ \frac{\langle 0|L_y|n\rangle \langle n \left|\frac{2L_y}{r^3}\right| 0\rangle}{(E_n - E_0)} + \frac{\langle 0 \left|\frac{2L_y}{r^3}\right| n\rangle \langle n|L_y|0\rangle}{(E_n - E_0)} \right\} \quad (3)$$

Where L_x, L_y and L_z are the components of angular momentum along the x, y and z axes respectively. The first part of these three equations originates from the spherical distribution of electronic changes when the electrons are in s orbital state. The second term comes from the distortion of spherical charge distribution when electrons are in p orbital state. In liquid-state NMR spectroscopy, due to the random motion of the molecule, the off-diagonal term of CSA tensor is averaged out and only the diagonal components survive.[29]

The CSA tensor can be determined by solid-state NMR techniques like two dimensional MAS/CSA NMR experiment;[30] SUPER (separation of undistorted powder patterns by effortless recoupling);[31] ROCSA (recoupling of chemical shift anisotropy);[32] RNCSA(γ-encoded RN_n^ν-symmetry based chemical shift anisotropy);[33] 2DMAF (Two-dimensional magic angle flipping) experiment;[34-36] 2DMAT (two-dimensional magic angle turning) experiment.[37] 2DPASS CP-MAS (two-dimensional phase adjusted spinning sideband cross-polarization magic angle spinning) SSNMR experiment[38,39] was developed to separate anisotropic and isotropic chemical shift interactions under low magic angle spinning (MAS) frequency using sequences of five π pulses. The correlation between the structure and dynamics of biopolymer and drugs molecules[40-51] were studied by measuring principal components of CSA parameters and site specific spin-lattice relaxation time by applying 2DPASS CP-MAS SSNMR experiments[38,39] and Torchia CP experiment[52] respectively. The main focus of the present work is to study the structure and dynamics of antifungal agent ketoconazole by the 2DPASS CP-MAS SSNMR experiments[38,39] and the Torchia CP

experiments.[52] The molecular correlation time at crystallographically different carbon sites of ketoconazole is also calculated by considering that the spin-lattice relaxation mechanism for ^{13}C carbon is mainly governed by hetero-nuclear dipole-dipole coupling and CSA-interaction. These types of investigations will provide a vivid picture about the structure and dynamics of ketoconazole, which will help to develop advanced antifungal drugs.

2. Experimental

2.1 NMR- Measurements

The active pharmaceutical ingredient of ketoconazole was purchased from Sigma Aldrich. ^{13}C CP-MAS solid-state NMR experiments were performed on a JEOL ECX 500 NMR spectrometer. The resonance frequency for the ^{13}C nucleus was 125.721 MHz. All the experiments were performed by using a 3.2 mm JEOL double resonance MAS probe. The MAS frequency for the ^{13}C CP-MAS NMR experiment was 10 kHz. Contact time for Cross-Polarization (CP) was 2 ms, with a repetition interval of 30 s, and SPINAL-64 ^{1}H decoupling at 3072 accumulations time. ^{13}C spin-lattice relaxation experiment was performed by using the Torchia CP method with contact time 2ms.[52]

2.2 CSA-Measurements

The analysis of static ^{13}C solid-state NMR spectrum encounters considerable difficulties because anisotropic interactions give rise to a broad powder-pattern and a considerable loss of sensitivity compared to ^{13}C liquid state NMR spectrum. Besides, the spin-lattice relaxation time of the ^{13}C nucleus of some organic compounds is extremely large, which makes the experiments unreasonably long. ^{13}C CP-MAS SSNMR experiment removes anisotropic interactions of the second rank and the spin-lattice relaxation time of proton is considerably fast. Hence, the ^{13}C CP-MAS SSNMR experiment enhanced the sensitivity, decrease the duration of the experiment, and make to spectrum simple. But the information about the three-dimensional molecular conformation and local electronic distribution surrounding a

nucleus is lost, because all these informations are encoded in the anisotropic interactions. The chemical shift anisotropy (CSA) parameters can be restored by reducing the magic angle spinning (MAS) frequency less than the span of the chemical shift anisotropy. In that condition, the solid-state NMR spectra contain sets of sidebands spaced in MAS frequency.[53,54] ^{13}C 2DPASS CP-MAS SSNMR experiments[38,39] can extract the CSA parameters by manipulating spinning sidebands. Chemical shift anisotropy (CSA) tensor can be extracted by using the intensities of these spinning sidebands by incorporating Herzfeld and Berger method.[55] This experiment is preferable compared to two-dimensional magic angle flipping (2DMAF) experiment,[35,36] and two-dimensional magic angle turning (2DMAT) experiment[37] due to the following reasons. To achieve the flipping of the magic angle during one experiment in 2DMAF experiment, it is required a complicated probe design. On the other hand, 2DMAT is not a constant time experiment, so it would be difficult to extract CSA information from the two-dimensional spectrum.

The pulse sequence of the 2DPASS experiment with five π pulses was introduced by Antzutkin et al.[38] The time duration of the PASS sequence is constant and the time gap among five π pulses varied according to the PASS equations. The 2DPASS CP MAS NMR experiments were carried out at two MAS frequencies 600 Hz and 2000 Hz. The contact time was 2ms to maintain CP condition. The 90 degree pulse length for ^{13}C nucleus was 3 us.

3. Determination of Chemical Shift Anisotropy Parameter:

The chiral drug ketoconazole is a racemic (1:1) mixture of enantiomers of the cis configuration.[3,4] The chemical formula of this imidazole derivative is cis-1-acetyl-4-[4-[[2-(2,4-dichlorophenyl)-2-(1H-imidazol-1-ylmethyl)-1,3-dioxolan-4-yl]methoxy]phenyl]piperazine). It is insoluble in water. It is a weak base with pKa values of 6.51 and 2.94. Figure 1 (a) shows the chemical structure of ketoconazole molecule, which is associated with the rich aromatic molecular moieties like N-acetylpiperazine phenyl group,

1,3 dioxolane ring, imidazole ring, and dichlorophenyl ring. The piperazine rings have chair conformations, and the benzene ring is distorted because three atoms of the ring are split on the basis of their thermal parameters.[56,57] Phenylpiperazine ring has no contribution to interact with the heme group CYP51, it interact with amino acid residues in the substrate access channel. The conformations of the 1,3-dioxolane rings are halfway between an envelope with flap at the unsubstituted carbon atom.[56,57] Stereochemical orientation of the dioxolane ring plays a vital role in the inhibition of the hedgehog signalling pathway and it is also responsible for inhibition of CYP3A4 to thwart coordination of the molecular oxygen, essential for oxidation.[58-60] The imidazole and the 2,4-dichlorobenzene rings have planar conformation.[56,57] The antifungal action of the azole group keteconazole is due to the binding of the imidazole nitrogen with cytochrome P45051.[58-61] The ketoconazole drug is entrenched in the hydrophobic region. The lipid-drug complex is fabricated by the action of the van der Waals type of interactions and electrostatic interaction.[62] Figure 1(b) shows the ^{13}C CP-MAS SSNMR spectrum of ketoconazole. Isotropic chemical shift is highest for those carbon nuclei which are in sp^2 hybridization and bonded with electronegative atoms oxygen, nitrogen, and chlorine. It is lowest for those carbon atoms which are in sp^3 hybridization like C2, C3, C4, C5 atoms reside on the piperazine ring, and the methyl group carbon C26.

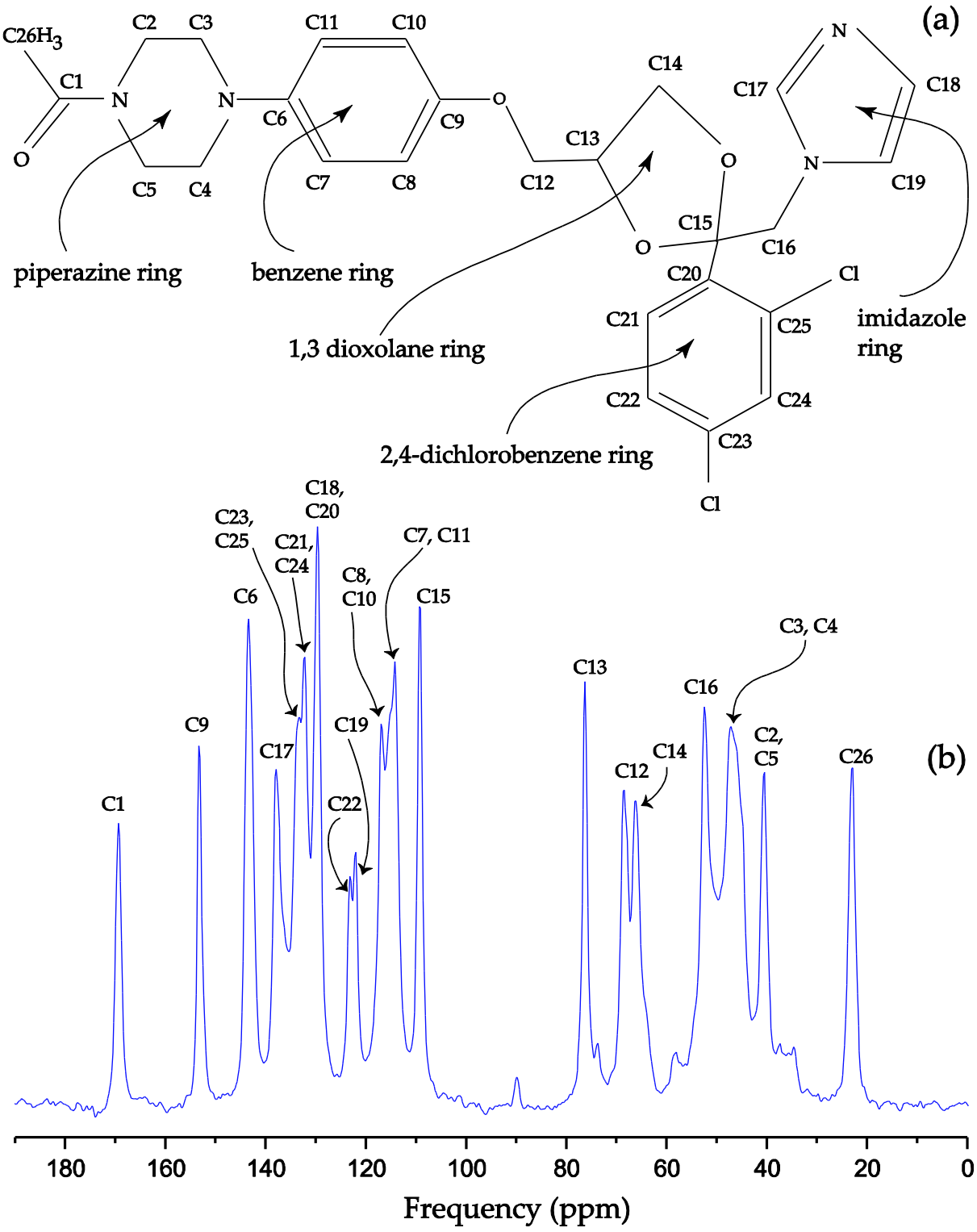

Figure 1: (a) Chemical structure of ketoconazole molecule. It is associated with five rings – piperazine ring, benzene ring, 1,3-dioxolane ring, imidazole ring, and 2,4-dichlorobenzene ring. It forms a close-pack arrangement by $\pi \ldots \pi$ stacking interaction. (b) ^{13}C CP-MAS NMR spectrum of ketoconazole.

Table1: Principal components CSA tensor of ketoconazole molecule

CSA parameters of ketoconazole molecule								
Carbon nuclei	δ_{11} (ppm)	δ_{22} (ppm)	δ_{33} (ppm)	Span (ppm) $\Omega = \delta_{11} - \delta_{33}$	Skew $k = \frac{3(\delta_{22} - \delta_{iso})}{\Omega}$	δ_{iso} (ppm)	Anisotropy (ppm) $\Delta\delta = \delta_{33}$- $\frac{(\delta_{11} + \delta_{22})}{2}$	Asymmetry $\eta = \frac{\delta_{22} - \delta_{11}}{\delta_{33} - \delta_{iso}}$
C1	240.69	171.37	95.83	144.85	0.04	169.3	-110.2	0.9
C9	231.36	150.18	78.05	153.3	-0.06	153.2	117.2	0.9
C6	222.07	137.57	70.64	151.43	-0.1	143.4	117.9	0.85
C17	245.33	108.77	59.3	185.99	-0.46	137.8	161.3	0.46
C23 C25	231.97	128.46	41.26	190.7	-0.08	133.9	147.1	0.89
C21 C24	222.26	130.68	43.63	178.6	-0.02	132.2	135.1	0.97
C18 C20	208.28	128.57	51.64	156.64	-0.02	129.5	118.2	0.97
C22	189.25	133.04	47.19	142.05	0.2	123.16	-113.9	0.74
C19	189.63	130.69	46.22	143.41	0.18	122.18	-113.9	0.77
C8, C10	215.61	99.92	35.63	179.98	-0.3	117.05	147.8	0.65
C7, C11	218.35	90.47	33.56	184.79	-0.38	114.12	156.33	0.5
C15	134.74	109.27	83.88	50.86	0	109.3	38.17	1
C13	121.44	59.53	47.92	73.52	-0.68	76.3	67.7	0.2
C12	108.85	58.8	37.84	71.01	-0.41	68.5	60.5	0.5
C14	106.6	52.09	40.18	66.44	-0.64	66.3	60.5	0.3
C16	69.23	52.38	36.33	32.89	-0.02	52.6	24.87	0.97
C3, C4	59.49	48.05	34.96	24.52	0.06	47.5	-18.8	0.9
C2, C5	52.9	42.2	26.9	26	0.18	40.68	-20.7	0.77
C26	40.2	14.58	14.5	25.69	-1	23.1	25.66	0

Figure 2 shows the ^{13}C 2DPASS CP-MAS SSNMR spectrum of ketoconazole. The direct dimension represents the pure isotropic spectrum, and the indirect dimension represents the anisotropic spectrum. Table 1 shows the principal components of CSA parameters at numerous carbon nuclei sites of ketoconazole. Figure 3 and Figure 4 show the spinning CSA sideband pattern of various carbon nuclei reside on the imidazole ring and the side chain of ketoconazole molecule. The centre of gravity of the spinning CSA sideband pattern is the isotropic chemical shift$\left\{\delta_{iso} = \frac{\delta_{11}+\delta_{22}+\delta_{33}}{3}\right\}$. The resonance frequency of numerous carbon nuclei differs according to the electronic distribution and the orientation of the molecular moiety with respect to the external magnetic field. It is shifted towards the higher frequency side (δ_{11}) and the lower frequency (δ_{33}) side due to the deshielding effect and the shielding effect respectively. The third principal value (δ_{22}) of CSA tensor arises when the orientation of the molecular moiety is perpendicular to the axes of δ_{11} and δ_{33}.[29] The left and right edges of the spinning CSA sideband pattern corresponds to the largest (δ_{11}) and smallest (δ_{33}) chemical shift respectively. Whereas δ_{22} corresponds to the position of the maximum intensity of the CSA sideband pattern when $\delta_{11} \geq \delta_{22} \geq \delta_{33}$. The maximum width of the CSA pattern is defined as 'span' ($\Omega = \delta_{11} - \delta_{33}$). The asymmetry$\left(\eta = \frac{\delta_{22}-\delta_{11}}{\delta_{33}-\delta_{iso}}\right)$ parameter defines how much the CSA pattern deviates from its axially symmetric shape. If $\delta_{11} = \delta_{22}$ or $\delta_{22} = \delta_{33}$, then the CSA pattern is axially symmetric and the value of the asymmetry parameter is zero. The orientation of the asymmetry of the CSA pattern is represented by the parameter called 'skew' $k = \frac{3(\delta_{33}-\delta_{iso})}{\Omega}$. The spinning CSA sideband pattern is asymmetric for C1, C9, C6, C23, C25, C21, C24, C18, C20, C22, C19,C15, C16, C3, C4, C2, and C5 nuclei and it is axially symmetric for C26 nuclei. For C13 and C14 nuclei, the spinning CSA sideband patterns are nearly axially symmetric. The magnitude of the anisotropy$\left[\Delta\delta = \delta_{33} - \frac{(\delta_{11}+\delta_{22})}{2}\right]$ parameter measures the largest separation of spinning CSA sideband pattern from

the center of gravity. The sign of the anisotropy parameters says on which side of the certer of gravity, the separation is the largest. Figure 5 shows the bar-diagram of anisotropy and asymmetry parameter at numerous carbon nuclei sites of ketoconazole.

Ketoconazole molecule is chemically related to miconazole. The bioavailability of this antimycotic agent originates from its capability to penetrate the cell membrane due to the presence of the methyl group at C1 position(carbonyl group carbon).[63] The chemical shift is the highest for carbonyl group carbon. One of the reasons of the large value of CSA parameters of carbonyl group carbon is the magnetic anisotropy. There is no symmetry axis in the carbonyl group; naturally, there arise three different magnetic susceptibilities $\mathcal{X}_x, \mathcal{X}_y, \mathcal{X}_z$ along three mutually perpendicular directions of the principal axes system (PAS). There originate two anisotropic susceptibilities -one parallel to the magnetic field ($\Delta\mathcal{X}_{\parallel} = \mathcal{X}_z - \mathcal{X}_x$) and another perpendicular to the magnetic field ($\Delta\mathcal{X}_{\perp} = \mathcal{X}_y - \mathcal{X}_x$).[64] The McConnell equation[65] of magnetic anisotropy for non-symmetric carbonyl group is $\delta_{aniso} = \{\Delta\mathcal{X}_{\parallel}(3cos^2\theta_1 - 1) + \Delta\mathcal{X}_{\perp}(3cos^2\theta_2 - 1)\}/3R^3$, where θ_1 is the angle between the radius vector R and x-axis and θ2 is the angle between radius vector R and z-axis.[66] Large amount of directional dependent magnetic field is generated due to this highly anisotropic magnetic susceptibility. This manifests as a large value of anisotropic chemical shift.

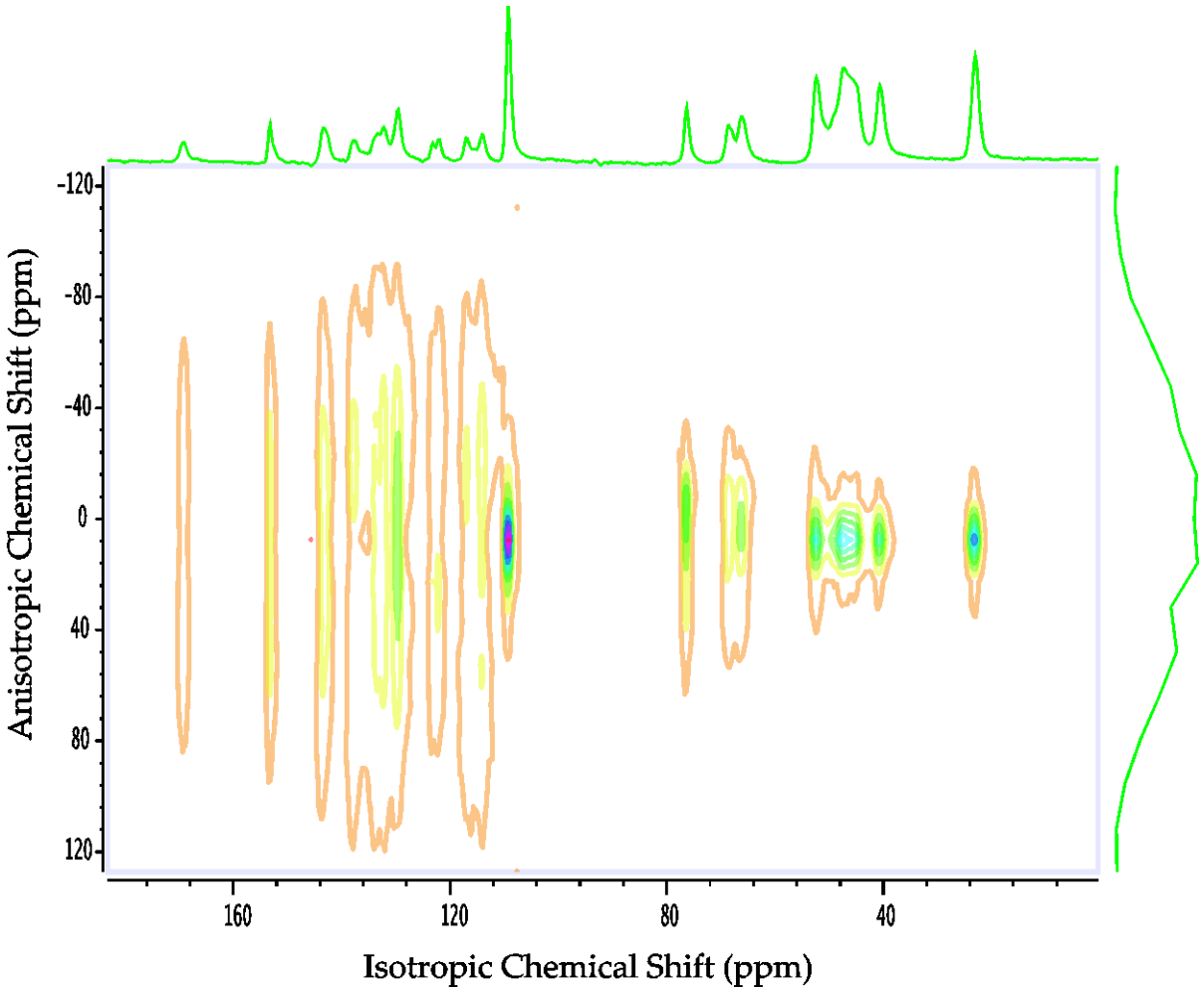

Figure 2: ^{13}C 2DPASS CP-MAS NMR spectrum of ketoconazole. Direct dimension represents infinite spinning speed spectrum, and the indirect dimension represents chemical shift anisotropy spectrum.

Among five rings of ketoconazole molecule, CSA parameters are very low for carbon nuclei (C2, C3, C4, C5) reside on the piperazine ring and the 1,3 dioxolane ring. But CSA parameters are very high for carbon nuclei reside on the benzene ring, imidazole ring, and the 2,4-dichlorobenzene ring due to the presence of π-electrons, which induced nonspherical distribution of electronic charge density on three rings. The existence of the π −electron surrounding the nucleus is responsible for the appearance of magnetic shielding and deshielding effect.[67] A paramagnetic current is generated when the π-electron circulates the nucleus in a clockwise direction and there induced a magnetic field along the direction of the

external magnetic field. As a consequence, the net magnetic field experienced by the nucleus is increased, which is known as the magnetic deshielding effect. On the other hand, when an π −electron revolves around the nucleus along the counter-clockwise direction, a magnetic field is generated along the opposite direction of the external magnetic field. As a consequence, the value of the net magnetic field is decreased, which is known as the magnetic shielding effect. These magnetic shielding and deshielding effects manifest themselves as a large value of chemical shift anisotropy. On the contrary, piperazine and 1,3 dioxolane rings are not associated with π −electrons, hence CSA parameters are not large for carbon nuclei reside on these two rings.

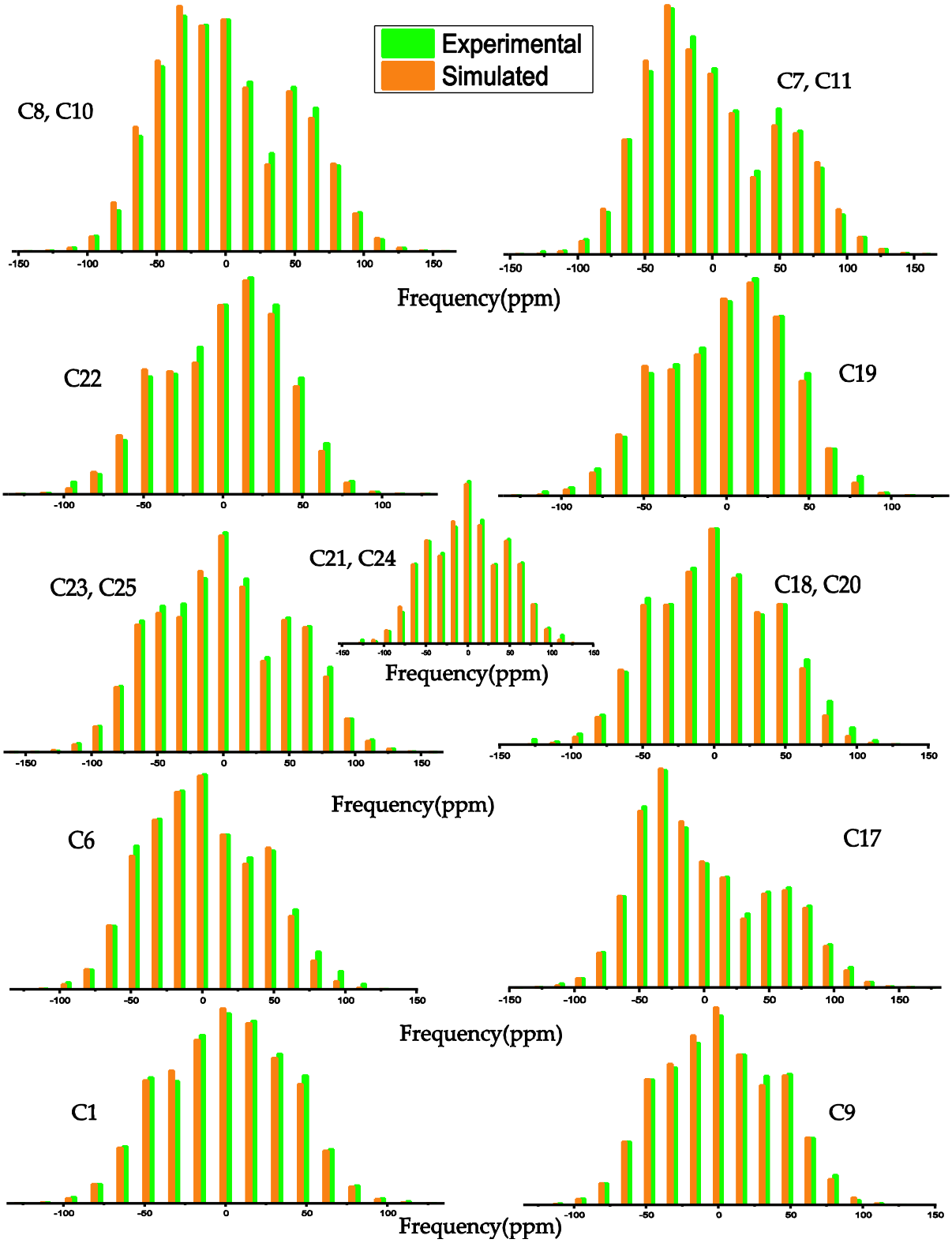

Figure 3: Spinning CSA sideband pattern of crystallographically different carbon sites of ketoconazole.

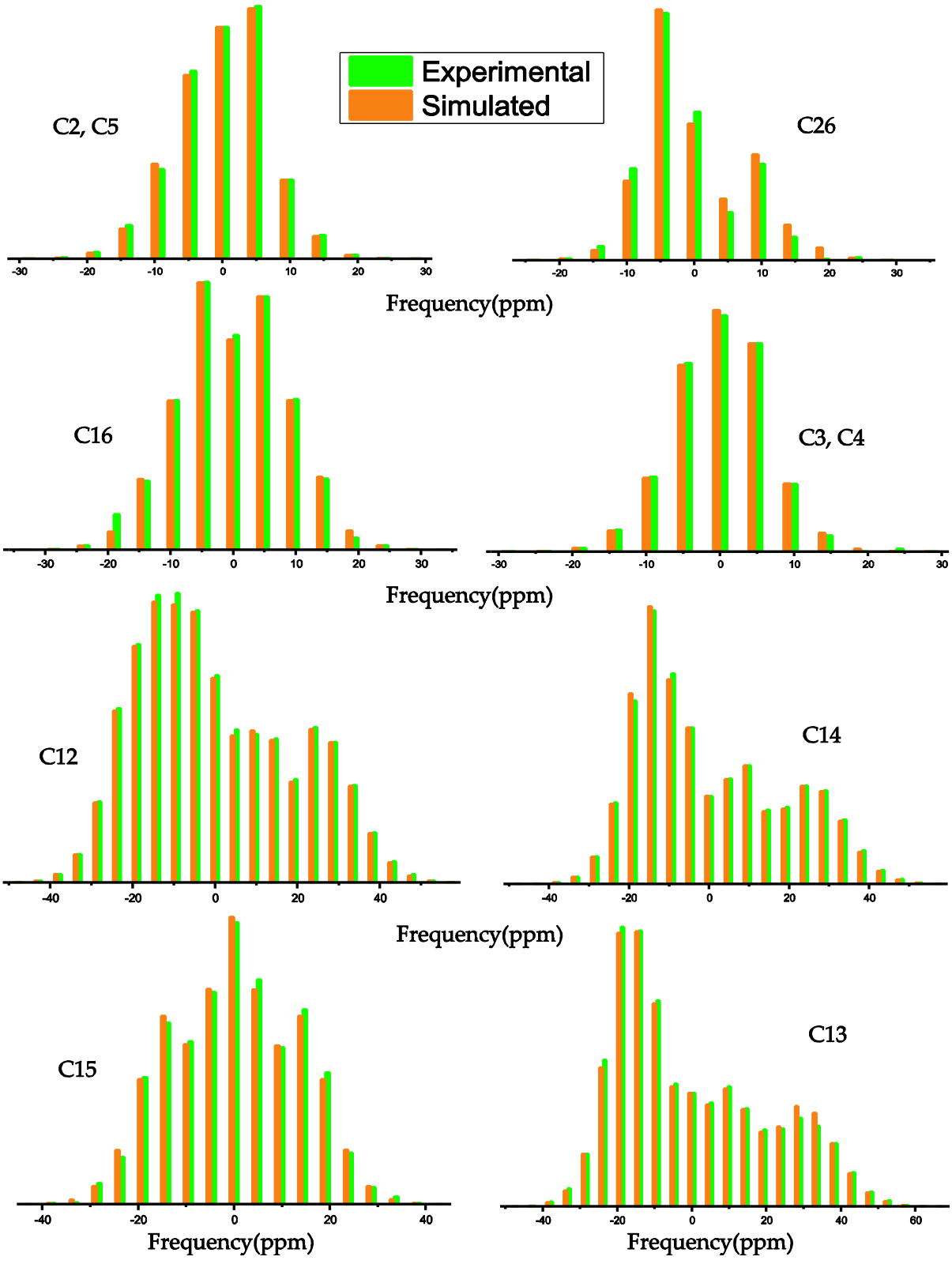

Figure 4: Spinning CSA sideband pattern of crystallographically different carbon sites of ketoconazole.

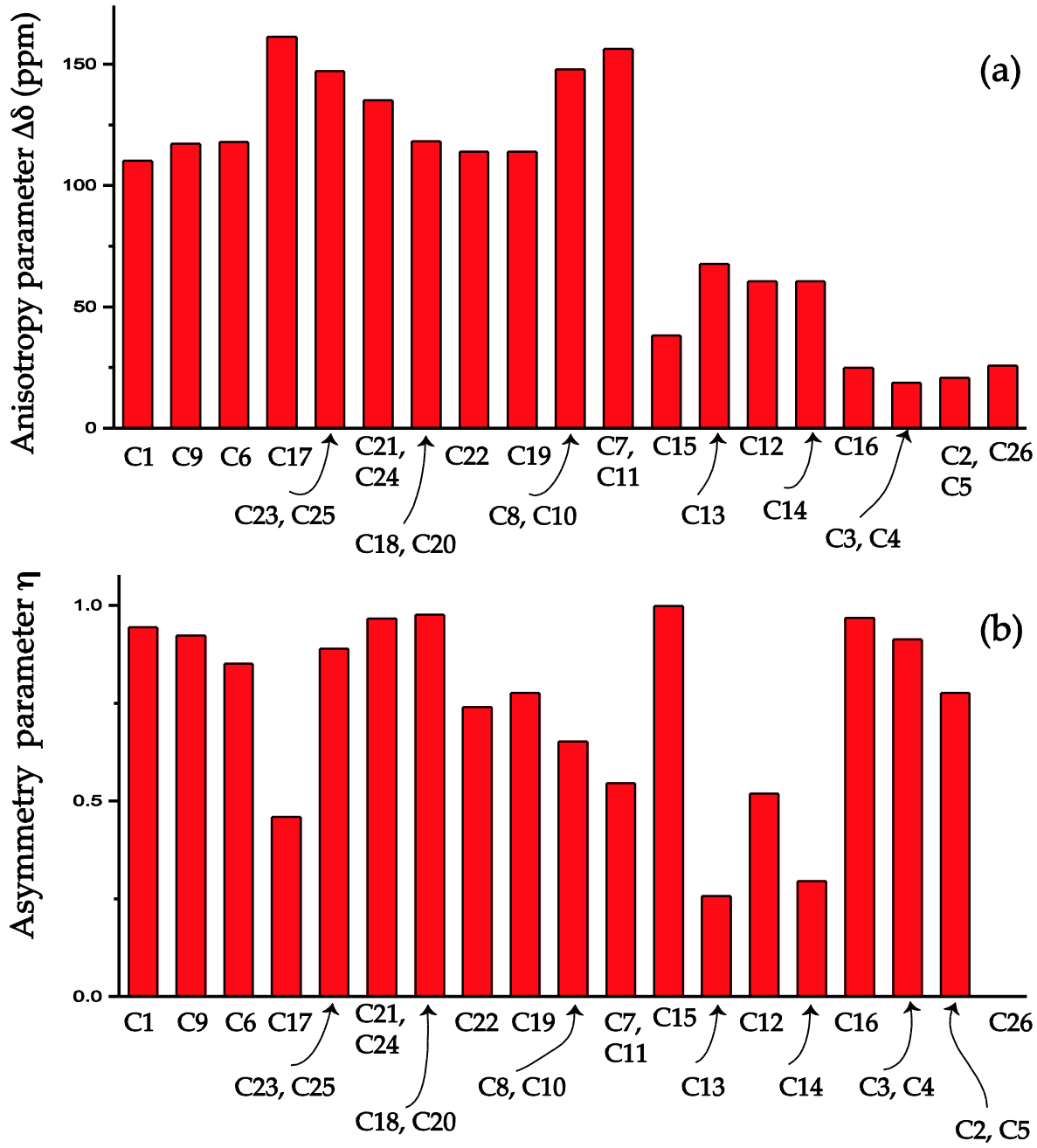

Figure 5: The bar-diagram of (a) anisotropy and (b) asymmetry parameter of ketoconazole.

Determination of Spin-lattice Relaxation Time and Molecular Correlation Time:

The dipole-dipole interaction, chemical shift anisotropy (CSA) interaction, spin-rotation interaction, scalar coupling, and the quadrupolar coupling play significant role in the spin-lattice relaxation mechanism. But for large molecules the contribution of spin-rotation interaction and scalar coupling is insignificant. Hence, for spin $1/2$ carbon nuclei, the spin-

lattice relaxation mechanism is mainly dominated by chemical shift anisotropy interaction and dipole-dipole coupling interaction. The contribution of chemical shift anisotropy interaction in spin-lattice relaxation mechanism is expressed as [68-71]

$$\frac{1}{T_1^{CSA}} = \frac{2}{15}\gamma^2 B^2 S^2 \left(\frac{\tau_2}{1 + \omega^2\tau_2^2}\right) \quad (4)$$

Where correlation time $\tau_c = 3\,\tau_2$ and B is the applied magnetic field. Where $S^2 = (\Delta\delta)^2(1 + \eta^2/3)$ and $\left[\Delta\delta = \delta_{33} - \frac{(\delta_{22}+\delta_{11})}{2}\right]$, $\left(\eta = \frac{\delta_{22}-\delta_{11}}{\delta_{33}-\delta_{iso}}\right)$.

The role of dipole dipole interaction in spin-lattice relaxation mechanism is expressed as[70]

$$\frac{1}{T_1{}^{DD}} = \frac{1}{10}\left(\frac{\gamma_C\gamma_X\hbar}{r_{CX}^3}\right)^2 \tau_2 \left[\frac{3}{1 + \omega_C{}^2\tau_2^2} + \frac{1}{1 + (\omega_X - \omega_C)^2\tau_2^2} + \frac{6}{1 + (\omega_X + \omega_C)^2\tau_2^2}\right] \quad (5)$$

By keeping only the first term,

$$\frac{1}{T_1{}^{DD}} = \frac{1}{10}\left(\frac{\gamma_C\gamma_X\hbar}{r_{CX}^3}\right)^2 \tau_2 \left[\frac{3}{1 + \omega_C{}^2\tau_2^2}\right] \quad (6)$$

Where X represents hydrogen, oxygen, chlorine and nitrogen atoms. r_{CX} is the distance between carbon and the nearest neighbour atoms like hydrogen, oxygen, nitrogen, chlorine. The bond-distance is calculated by X-ray crystallography study.[56,57] Larmor precession frequency of carbon nucleus is $\omega_c = 2\pi f = 2 \times 3.14 \times 125.758$ MHz = 789.76024 MHz. $B = 11.74\,T$, $\gamma_C = 10.7084$ MHz$/T$, $\gamma_H = 42.577$ MHz$/T$, $\hbar = 1.054 \times 10^{-34}\,Js$.

The spin-lattice relaxation rate for ^{13}C can be expressed as

$$\frac{1}{T_1} = \frac{1}{T_1^{CSA}} + \frac{1}{T_1^{DD}}$$

$$= \frac{2}{15}\gamma^2 B^2 S^2 \left(\frac{\tau_2}{1 + \omega^2\tau_2^2}\right)$$

$$+ \frac{1}{10}\left(\frac{\gamma_C \gamma_X \hbar}{r_{CX}^3}\right)^2 \tau_2 \left[\frac{3}{1 + {\omega_C}^2\tau_2^2}\right] \qquad (7)$$

Molecular correlation time is calculated by this equation.

Table 2: Spin-lattice relaxation time and molecular correlation time of ketoconazole

Carbon Nuclei	Spin-lattice relaxation time (s)	Molecular Correlation time (s)
C1	500 ± 15	6.3×10^{-4}
C9	480 ± 12	6.7×10^{-4}
C6	262 ± 5	3.6×10^{-4}
C17	374 ± 10	8.3×10^{-4}
C23, C25	385 ± 10	8.4×10^{-4}
C21,C24	455 ± 10	8.7×10^{-4}
C18,C20	335 ± 10	4.9×10^{-4}
C22	280 ± 5	3.4×10^{-4}
C19	272 ± 5	3.4×10^{-4}
C8,C10	211 ± 5	4.2×10^{-4}
C7,C11	215 ± 5	4.6×10^{-4}
C15	412 ± 10	6.4×10^{-4}
C13	323 ± 5	1.2×10^{-4}
C12	250 ± 5	7.9×10^{-5}
C14	353 ± 5	1×10^{-4}

C16	213 ± 5	1.4×10^{-5}
C3, C4	8 ± 2	2.9×10^{-7}
C2, C5	12 ± 2	4.9×10^{-7}
C26	9 ± 2	4.7×10^{-7}

Figure 6 shows the longitudinal magnetization decay curves at (a) C1, (b) C9, (c) C6, and (d) C23, C25 nuclei sites of ketoconazole molecule. Figure 6(e) shows the bar-diagram of the spin-lattice relaxation time at chemically different carbon nuclei sites. From Table 2, it is clear that the spin-lattice relaxation rate is slow for the carbon nuclei reside on imidazole ring, 1,3 dioxolane ring, benzene ring, and 2, 4-dichlorobenzene ring. It suggests the close-pack arrangement of the molecule due to $\pi - \pi$ stacking interaction.[61,72] As it is mentioned before, the CSA parameters of the carbon nuclei reside on these four rings are larger compared to the carbon nuclei C2, C3, C4, C5 and C26 reside on the piperazine ring and the methyl group respectively. The spin-lattice relaxation rate is fast for C2, C3, C4, C5 and C26 carbon nuclei. The 1,3-dioxolane ring is responsible for inhibition of CYP3A4 to thwart coordination of the molecular oxygen, essential for oxidation. The stereochemical orientation of the 1,3-dioxolane ring plays a significant role in inhibition of the hedgehog signalling pathway.[61,72] Spin-lattice relaxation time of C17, C18, and C19 carbon nuclei reside on dioxolane ring is 374s, 335s and 272s respectively. The molecular correlation time is 8.3×10^{-4}s, 4.9×10^{-4}s and 3.4×10^{-4} s for C17, C18 and C19 respectively. The values of the CSA parameters are very large. The keto group is located in the polar pocket in ketoconazole molecule.[61] The spin-lattice relaxation time is longest (500 s) for C1 carbon reside on keto group. Both the values of isotropic chemical shift and anisotropic chemical shift are also highest for C1. Table 2 shows that the molecular correlation time of all the carbon atoms reside on the benzene ring, 1,3-dioxolane ring, imidazole ring, and the 2,4-dichlorobenzene ring is of the order of 10^{-4} s, while it is of the order of 10^{-7} s for carbon

atoms reside on the piperazine ring and the methyl group. Hence, motional degrees of freedom of the carbon nuclei reside on the piperazine ring are much higher than those who reside on the other four rings of ketoconazole. As it was mentioned before that the piperazine rings have chair conformations, and it has no contribution to interact with the heme group CYP51. It interacts with amino acid residues in the substrate access channel. The antifungal action of the azole group ketoconazole is due to the binding of the imidazole nitrogen with cytochrome P45051. The CSA parameters of those carbon nuclei (C2, C3, C4, C5) reside on the piperazine ring is also very low compared to those carbons reside on the other four rings. The long side-chain of ketoconazole played a vital role in adjusting the physicochemical properties of the molecule to improve the pharmacokinetic and pharmacodynamic behavior. The CSA parameters are very high for carbon nuclei reside on the side-chain of the molecule like benzene ring, imidazole ring, and the 2,4-dichlorobenzene ring due to the presence of π-electrons. Figure 6(e) and Figure 7 show a substantial variation of the motional degrees of freedom of side-chain carbon nuclei. The spin-lattice relaxation time varies from 500 s to 8 s; and the molecular correlation time varies in the range of 10^{-4}s to 10^{-7}s.

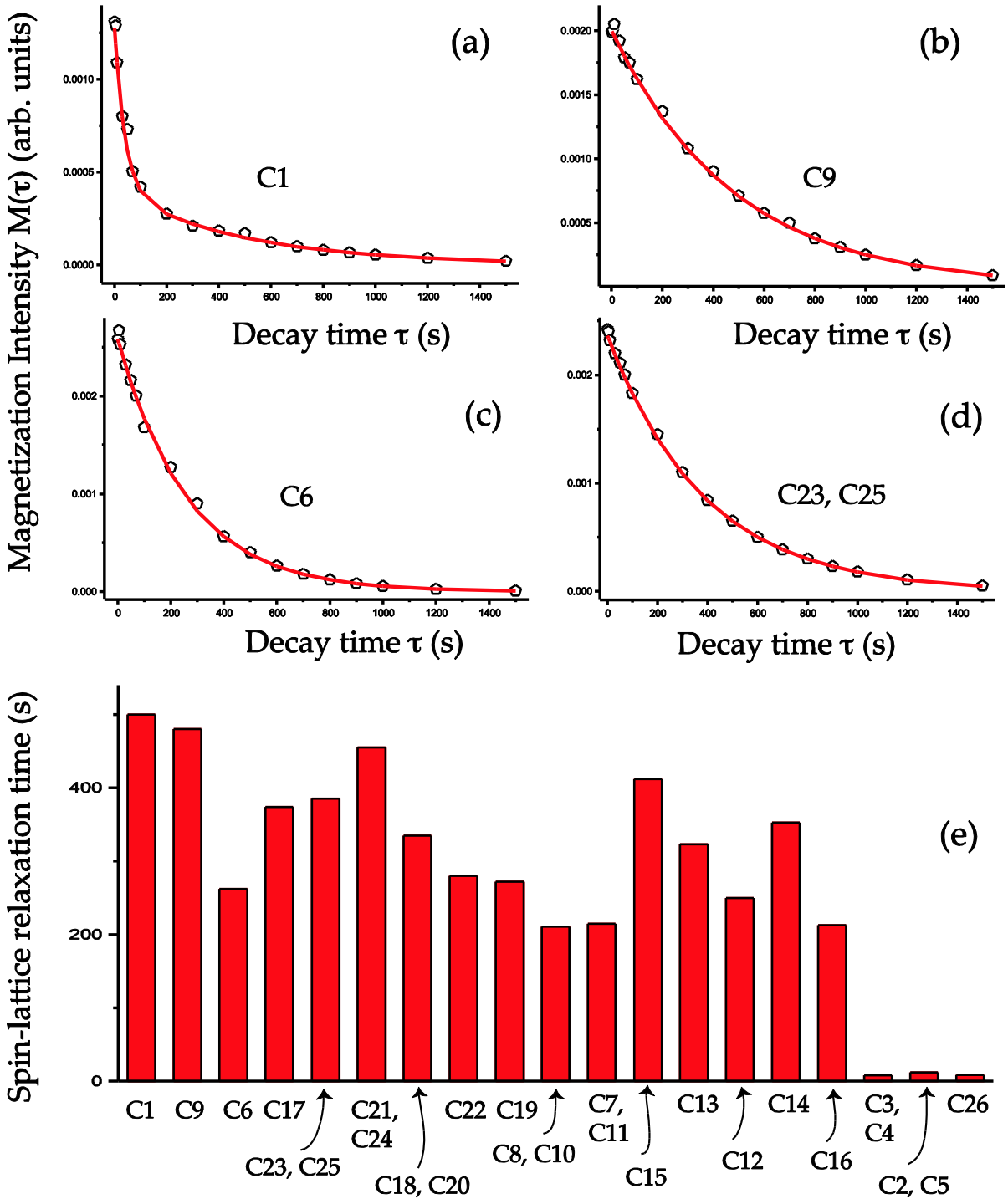

Figure 6: The longitudinal magnetization decay curves at (a) C1, (b) C9, (c) C6, and (d) C23, C25 nuclei sites of ketoconazole. (e) Bar-diagram of spin-lattice relaxation time at chemically different carbon nuclei sites of ketoconazole.

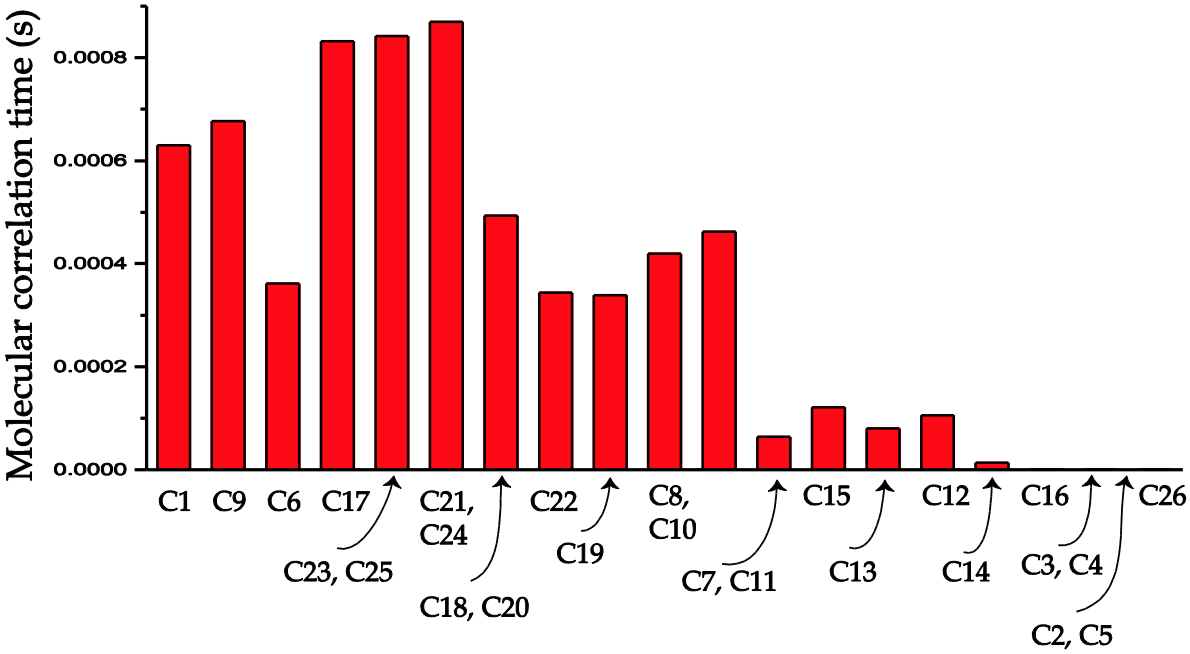

Figure 7: Bar-diagram of molecular correlation time at various carbon nuclei sites of ketoconazole.

4. Conclusion:

A lipophilic imidazole derivative, ketoconazole, is used for the treatment of mucosal fungal infections associated with AIDS immunosuppression, organ transplantation, and cancer chemotherapy. The structure and dynamics of ketoconazole have been explored by measuring chemical shift anisotropy tensor, site-specific spin-lattice relaxation time, and by calculating the molecular correlating time at the crystallographically different carbon sites. The CSA parameters at the crystallographically distinct site of ketoconazole were determined by two-dimensional phase adjusted spinning sideband (2D PASS) cross-polarization magic angle spinning (CP-MAS) solid-state NMR experiment. The site-specific spin-lattice relaxation time was determined by the Torchia CP method. The values of CSA parameters are large for the carbon nuclei involved in sp^2 hybridization and bonded with electronegative oxygen, nitrogen, and chlorine atoms. The presence of π-electrons induced nonspherical distribution of electronic charge density surroundings the carbon nuclei, which leads to the higher values

of the CSA parameters. On the contrary, CSA parameters are lower for the carbon nuclei reside on the piperazine ring, 1,3-dioxolane ring, and the methyl group i.e. for those carbon which are in sp^3 hybridization. The spin-lattice relaxation rate is faster for the carbon nuclei C2, C3, C4, C5, and C26, whose CSA parameters are lower compared to other carbon nuclei of ketoconazole molecule. On the other hand, the spin-lattice relaxation rate is slower for the carbon nuclei reside on the benzene ring, 1,3-dioxolane ring, imidazole ring, and the 2,4-dichlorobenzene ring and the keto group of ketoconazole. The CSA parameters of those carbon nuclei are also very large. This suggests the close-pack arrangement of the molecule due to the $\pi - \pi$ stacking interaction. The molecular correlation time of all the carbon atoms reside on the benzene ring, 1,3-dioxolane ring, imidazole ring, 2,4-dichlorobenzene ring, and the keto group is of the order of 10^{-4} s, while it is of the order of 10^{-7} s for carbon nuclei reside on the piperazine ring. Hence, motional degrees of freedom of the carbon nuclei reside on the piperazine ring are much higher than those who reside on the other four rings of ketoconazole. The piperazine rings have chair conformations, and it has no contribution to interact with the heme group CYP51. It interacts with amino acid residues in the substrate access channel. The antifungal action of the azole group ketoconazole is due to the binding of the imidazole nitrogen with cytochrome P45051. The CSA parameters are very large for the carbon nuclei reside on the imidazole ring. The spin-lattice relaxation rate is slow, and the molecular correlation time is of the order of 10^{-4}s. The long side chain of ketoconazole played a vital role in adjusting the physicochemical properties of the molecule to improve the pharmacokinetic and pharmacodynamic behaviour. The CSA parameters are very high for carbon nuclei reside on the side-chain of the molecule like benzene ring, imidazole ring, and the 2,4-dichlorobenzene ring due to the presence of π-electrons. A remarkable variation of the motional degrees of freedom is observed for side-chain carbon nuclei. The spin-lattice relaxation time varies from 500 s to 8 s; and the molecular correlation time varies in the range

of 10^{-4}s to 10^{-7}s. These types of in-depth analysis of the structure and dynamics of the azole class antifungal agent will help to develop advanced antifungal drugs. Additionally, the CSA information of the drug molecules will be immensely useful for NMR crystallography.

Acknowledgements

The author Manasi Ghosh is grateful to Science and Engineering Research Board (SERB), Department of Science and Technology (DST), Government of India(file no. EMR/2016/000249) for financial support.

Reference:

1. Beggs WH (1991) Protonation of ketoconazole in relation to fungistatic activity. Mycopathologia 116(1): 3-4.
2. Skiba M, Skiba-Lahiani M, Marchais H, Duclos R, and Arnaud P (2000) Stability assessment of ketoconazole in aqueous formulations. Int J Pharm 198(1): 1-6.
3. Hamdy DA and Brocks DR (2008) A stereospecific high-performance liquid chromatographic assay for the determination of ketoconazole enantiomers in rat plasma. Biomed Chromatogr 22(5): 542-547.
4. Hamdy DA and Brocks DR (2010) High performance liquid chromatographic assay for the simultaneous determination of midazolam and ketoconazole in plasma. J Pharm Biomed Anal 53(3): 617-622.
5. Ginsburg CM, McCracken GH-Jr, and Olsen K (1983) Pharmacology of ketoconazole suspension in infants and children. Antimicrob Agents Chemother 23(5): 787-789.
6. Perez H (2004) Ketoconazole as an adjunct to finasteride in the treatment of androgenetic alopecia in men. Med Hypotheses 62(1): 112-115.
7. Wang L and Tang X (2008) A novel ketoconazole bioadhesive effervescent tablet for vaginal delivery: design, in vitro and 'in vivo' evaluation. Int J Pharm 350(1-2): 181-187.
8. Chander Shekar B, Shireesh Kiran R, and Nagendra Babu B (2010) Preparation and evaluation of gastro retentive floating tablets of ketoconazole. IJPRD 2(9): 174-184.
9. Kaur IP and Kakkar S (2010) Topical delivery of antifungal agents. Expert Opin Drug Deliv 7(11): 1303- 1327.
10. Patel GM and Patel AP (2010) A novel effervescent bioadhesive vaginal tablet of ketoconazole: formulation and in-vitro evaluation. Int J PharmTech Res 2(1): 656-667.
11. Agrawal TK and Murti Y (2011) Synthesis and bioevaluation of ketoconazole thiosemicarbazone analogues. IJPSR 2(12): 3156-3160.
12. Patel MH, Patel AM, Patel SM, Ninama GL, Patel KR, and Lavingia BC (2011) Antifungal susceptibility testing to determine MIC of amphotericine B, fluconazole and ketoconazole against ocular fungal infection. NJCM 2(2): 302-305.

13. Patel MR, Patel RB, Parikh JR, Solanki AB, and Patel BG (2011a) Investigating effect of microemulsion components: in vitro permeation of ketoconazole. *Pharm Dev Technol* 16(3): 250-258.
14. Rao Purushotham K, Venkateshwarlu P, Shashikala P, Sagare P, Saran SV, Ravindranath A, Ashok Kumar C, Anand C, and Jayanthi C (2012) Ketoconazole derma sticks for topical applications. Int J Res Chem Environ 2(1): 255-259.
15. Xin C, Li-hong W, Jing Y, Yang Y, Yue Y, Qi-fang W, and San-ming L (2012) Ketoconazole ion-exchange fiber complex: a novel method to reduce the individual difference of bioavailability in oral administration caused by gastric anacidity. *Pharm Dev Technol* doi: 10.3109/dmd.10837450.2012.696266
16. Abou-Attia FM, Issa YM, Abdel-Gawad FM, and Abdel-Hamid SM (2003) Quantitative determination of some pharmaceutical piperazine derivatives through complexation with iron(III) chloride. Farmaco 58(8): 573-579.
17. S. Dilmaghanian, J. G. Gerber, S. G. Filler, A. Sanchez, J. Gal, Enantioselectivity of Inhibition of Cytochrome P450 3A4 (CYP3A4) by Ketoconazole: Testosterone and Methadone as Substrates, *Chirality* 2004, **16**:79–85.
18. Rotstein DM, Kertesz DJ, Walker KAM, Swinney DC. Stereoisomers of ketoconazole: preparation and biological activity. *Journal of Medicinal Chemistry* 1992; 35:2818 – 2825.
19. S. Sen, Dynamics in Inorganic Glass-forming Liquids by NMR Spectroscopy, *Progress in Nuclear Magnetic Resonance Spectroscopy* (2019), doi: https://doi.org/10.1016/j.pnmrs.2019.11.001.
20. Antzutkin O. N. Sideband manipulation in magic-angle-spinning nuclear magnetic resonance. *Progress in Nuclear Magnetic Resonance Spectroscopy* 1999, 35: 203–266.
21. Ando I., Kuroki S., Kurosu H., Yamanobe T. NMR chemical shift calculations and structural characterizations of polymers. *Progress in Nuclear Magnetic Resonance Spectroscopy* 2001, 39 : 79-133.
22. Angel C. de Dios. Ab initio calculations of the NMR chemical shift. *Journal of Progress in Nuclear Magnetic Spectroscopy* 1996, 29 : 229–278.
23. Shao L., Titman J. J. Chemical shift anisotropy amplification. *Progress in Nuclear Magnetic Resonance Spectroscopy* 2007, 51 : 103–137.
24. Sitkoff D., Case D. A. Theories of chemical shift anisotropies in proteins and nucleic acids. *Progress in Nuclear Magnetic Resonance Spectroscopy* 1998, 32 :165-190.
25. Veeman W. S. Carbon-13 Chemical shift anisotropy. *Progress in Nuclear Magnetic Resonance Spectroscopy* 1984, 16:193-235.
26. Wylie B. J., Rienstra C. M. Multidimensional solid state NMR of anisotropic interactions in peptides and proteins. *The Journal of Chemical Physics* 2008, 128 : 052207.
27. Ramsey N. F. Magnetic Shielding of Nuclei in Molecules, *Physical Review* 1950, 78: 699-703.
28. Ramsey N. F. Chemical effects in nuclear magnetic resonance and in diamagnetic susceptibility. *Physical Review* 1952, 86: 243-246.
29. Laws D. D., Bitter H-M. L., Jerschow A., Solid-State NMR Spectroscopic Methods in Chemistry, *Angewandte Chemie Internationak Edition* 2002, **41**, 3096 – 3129.

30. Tycko R., Dabbagh G., Mirau P. A. Determination of chemical shift anisotropy lineshapes in a two-dimensional magic angle spinning NMR experiment. *Journal of Magnetic Resonance* 1989; 85: 265-274.
31. Liu S. F., Mao J. D., Schmidt-Rohr K. A robust technique for two-dimensional separation of undistorted chemical shift anisotropy powder patterns in magic angle spinning NMR. *Journal of Magnetic Resonance* 2002; 155:15-28.
32. Chan J. C. C., Tycko R. Recoupling of chemical shift anisotropies in solid state NMR under high speed magic angle spinning and in uniformly ^{13}C labelled systems. *Journal of Chemical Physics* 2003; 118:8378-8389.
33. Hou G., Byeon In-Ja L., Ahn J., Gronenborn A. M. ,Polenova T. Recoupling of chemical shift anisotropy by R-symmetry sequences in magic angle spinning NMR spectroscopy. *Journal of Chemical Physics* 2012; 137:134201-134210.
34. Bax Ad, Szeverenyi N. M., Maciel G. E. Chemical shift anisotropy in powdered solids studied by 2D FT NMR with flipping of the spinning axis. *Journal of Magnetic Resonance* 1983; 55:494-497.
35. Bax AD, Szeverenyi N.M., Maciel G.E., Correlation of isotropic shifts and chemical shift anisotropies by two-dimensional Fourier-transform magic angle hopping NMR spectroscopy. *Journal of Magnetic Resonance* 1983; 52: 147-152.
36. Bax AD, Szeverenyi N.M., Maciel G.E. Chemical shift anisotropy in powdered solids studied by 2D FT CP/MAS NMR. *Journal of Magnetic Resonance* 1983; 51: 400-408.
37. Gan Z. High-resolution chemical shift and chemical shift anisotropy correlation in solids using slow magic angle spinning. *Journal of American Chemical Society* 1992; 114: 8307-8309
38. Antzutkin O.N., Shekar S.C., Levitt M.H. Two-dimensional sideband separation in magic angle spinning NMR. *Journal of Magnetic Resonance* A 1995; 115: 7-19.
39. Dixon W.T., Spinning-sideband-free and spinning-sideband-only NMR spectra in spinning samples. *The Journal of Chemical Physics* 1982; 77: 1800-1809.
40. Ghosh M., Sadhukhan S., Dey K. K. Elucidating the internal structure and dynamics of α-chitin by 2DPASS-MAS-NMR and spin-lattice relaxation measurements. *Solid State Nuclear Magnetic Resonance* 2019; 97:7-16.
41. Ghosh M., Prajapati B. P., Kango N., Dey K. K. A comprehensive and comparative study of the internal structure and dynamics of natural β-keratin and regenerated β-keratin by solid state NMR spectroscopy. *Solid State Nuclear Magnetic Resonance* 2019; 101: 1-11.
42. Ghosh M., Kango N., Dey K. K. Investigation of the internal structure and dynamics of cellulose by ^{13}C-NMR relaxometry and 2DPASS-MAS-NMR measurements. *Journal of Biomolecular NMR* 2019; 73: 601-616.
43. Dey K. K., Ghosh M. Understanding the effect of deacetylation on chitin by measuring chemical shift anisotropy tensor and spin lattice relaxation time. *Chemical Physics Letters* 2020; 738: 136782.
44. Dey K. K., Gayen S., Ghosh M. Investigation of the detailed internal structure and dynamics of itraconazole by solid-state NMR measurements, *ACS Omega*, 2019, **4**, 21627-21635.
45. Dey K. K, Gayen S., Ghosh M. Understanding the correlation between structure and dynamics of clocortolone pivalate by solid state NMR measurement. *RSC Advances* 2020; 10: 4310-4321.
46. Ghosh M., Gayen S., Dey K. K. An atomic resolution description of folic acid by solid state NMR measurements. *RSC Advances* 2020; 10: 24973-24984.

47. K. K. Dey, M. Ghosh, Determination of the Correlation between the Structure and Dynamics of Deflazacort by solid state NMR measurements, *New Journal of Chemistry*, 2020 , **44**, 18419-18430
48. K. K. Dey, M. Ghosh, Understanding the Structure and Dynamics of Anti-inflammatory Corticosteroid Dexamethasone by solid state NMR Spectroscopy, *RSC Advances, 2020, 10, 37564.*
49. K. K. Dey, M. Ghosh, Determination of Chemical Shift Anisotropy Tensor and Molecular Correlation Time of Proton Pump Inhibitor Omeprazole by Solid State NMR Measurements, *New Journal of Chemistry*, 2020, 44, 19393-19403
50. K. K. Dey, M. Ghosh, Investigation of the Structure and Dynamics of Antiviral Drug Adefovir Dipivoxil by Site-Specific Spin–Lattice Relaxation Time Measurements and Chemical Shift Anisotropy Tensor Measurements, ACS Omega, 2020,5, 29373
51. R. Bhowal, A. Balaraman, M. Ghosh, S. Dutta, K. K. Dey, D. Chopra, Probing Atomistic Behavior to Unravel Dielectric Phenomena in Charge Transfer Cocrystals, Journal of American Chemical Society, 143, 1024-1037, 2021.
52. Torchia, D.A. The measurement of proton-enhanced carbon-13 T1 values by method which suppresses artifacts. *Journal of Magnetic Resonance* 1978; 30: 613.
53. Walder B.J., Dey K.K., Kaseman D.C., Baltisberger J.H., Grandinetti P.J. Sideband separation experiments in NMR with phase incremented echo train acquisition. *The Journal of Chemical Physics* 2013; 138: 174203-1-174203-12.
54. Fayon F., Bessada C., Douy A., Massiot D. Chemical bonding of lead in glasses through isotropic vs anisotropic correlation: PASS shifted Echo. *Journal of Magnetic Resonance* 1999; **137**: 116-121.
55. Herzfeld J., Berger A.E. Sideband intensities in NMR spectra of samples spinning at the magic angle. *Journal of Chemical Physics* 1980; **73**: 6021-6030.
56. O. M. Peeters, N. M. Blaton, J. G. Gerber, J. Gal, (+)-cis-1-Acetyl-4-(4-{[(2R,4S)-2-(2,4-dichlorophenyl)-2-(1H-imidazol-1-ylmethyl)-1,3-dioxolan4yl]methoxy}phenyl)piperazine [(2R,4S)-(+)-ketoconazole], *Acta Crystallographica Section* E 2004, E60, o367-o369.
57. O. M. Peeters, N. M. Balton, C. J. De Ranter, cis- 1 - A cetyl-4-(4- { [2-(2,4-dichlorophenyl)- 2-(1 H- 1 -imidazolylmethyl)- 1,3-dio x olan-4-yl]methoxy}phenyl)piperazine: Ketoconazole. A Crystal Structure with Disorder, *Acta Crystallographica Section* B 1979, B35, 2461-2464.
58. Ji, H.; Zhang, W.; Zhou, Y.; Zhang, M.; Zhu, J.; Song, Y.; Lu, J.; Zhu, J. A three dimensional model of lanosterol 14α-demethylase of Candida albicans and its interactions with azole antifungals. J. Med. Chem. 2000, 43, 2493−2505.
59. Odds, F. C.; Brown, A. J. P.; Gow, N. A. R. Antifungal agents: mechanisms of action. Trends Microbiol. 2003, 11, 272−279.
60. Dunmire, D.; Freedman, T. B.; Nafie, L. A.; Aeschlimann, C.; Gerber, J. G.; Gal, J. Determination of the absolute configuration and solution conformation of the antifungal agents ketoconazole, itraconazole, and miconazole with vibrational circular dichroism. *Chirality* 2005, 17, S101−S108

61. M. Ekroos and T. Sjo¨ gren, Structural basis for ligand promiscuity in cytochrome P450 3A4, *The Proceedings of the National Academy of Science* , 2006,**103**, 13682–13687.
62. B. Pawar, M. A. Kanyalkar, R. Pissurlenkar, M. Joshi, E. C. Coutinho, S. Srivastava, Probing molecular level interaction of antifungal drugs with model membranes by molecular modelling, multinuclear NMR and DSC methods, *International Journal of Current Pharmaceutical Research*, 2010, 2, 47-56.
63. Van den Bossche, H., Willemsens, G., Cools, W., Cornelissen, F., Lauwers, W. F. & Van Cutsem, J. (1980). In Vitro and In Vivo Effects of the Antimycotic Drug Ketoconazole on Sterol Synthesis. Antimicrobial Agents Chemotherapy, 17, 922-928.
64. R. J. Abraham,M. Mobli and R. J. Smith, (2003). 1H chemical shifts in NMR: Part 19† Carbonyl anisotropies and steric effects in aromaticaldehydes and ketones. *Magnetic Resonance in Chemistry*, 41, 26-36.
65. McConnell H.M., 1957. Theory of Nuclear Magnetic Shielding in Molecules: Long-Range Dipolar Shielding of protons. *The Journal of Chemical Physics*, 27, 226
66. Abraham R.J., Mobli M., Smith R.J., 2003. 1H chemical shifts in NMR : Carbonyl anisotropies and steric effect in aromatic aldehydes and ketones. *Magnetic Resonance in Chemistry*, 41, 26-36.
67. M. Randic , M. Novic and D. Plavsic , π-Electron currents in fixed π-sextet aromatic benzenoids, *J. Math. Chem.*, 2012, **50** , 2755 —2774
68. Orendt A. M., Facelli J. C. Solid state effects on NMR chemical shifts. *Annual Report NMR Spectroscopy* 2007; 62:115-178.
69. Tjandra N., Szabo A., Bax Ad. Protein backbone dynamics and 15B chemical shift anisotropy from quantitative measurement of relaxation interference effects. *Journal of American Chemical Society* 1996, 118(29): 6986 - 6991.
70. Dais P., Spyros A. ^{13}C nuclear magnetic relaxation and local dynamics of synthetic polymers in dilute solution and in the bulk state. *Progress in Nuclear Magnetic Resonance Spectroscopy* 1995, 27: 555-633.
71. Nicholas M. P., Eryilmaz E., Ferrage F., Cowburn D., Ghose R. Nuclear spin relaxation in isotropic and anisotropic media. *Progess in Nuclear Magnetic Resonance Spectroscopy* 2010, 57: 111-158.
.
72. Haitao Ji, Wannian Zhang, Youjun Zhou, Min Zhang, Jie Zhu, Yunlong Song, Jiaguo Lu¨ , and Ju¨ Zhu, A Three-Dimensional Model of Lanosterol 14r-Demethylase of Candida albicans and Its Interaction with Azole Antifungals, *Journal of Medicinal Chemistry*, 2000, **43**:2493-2505.
73. Talele, T. T.; Kulkarni V. M. Three-dimensional quantitative structure-activity relationship (QSAR) and receptor mapping of cytochrome P-45014RDM inhibiting azole antifungal agents. J. Chem. Inf. Comput. Sci. 1999, 39, 204-210.